Iranian Journal of Chemical Engineering

Journal Homepage: www.ijche.com

pISSN: 1735-5397
eISSN: 2008-2355

Regular Article

High-Performance Hydroxyapatite Scaffold Combined with Selenium and Reduced Graphene Oxide for Bone Regeneration Applications

Y. Beygi-Khosrowshahi [1*], ***S. Zakhireh*** [2]

[1] *Department of Chemical Engineering, Faculty of Engineering, Azarbaijan Shahid Madani University, Tabriz, Iran*
[2] *Drug Applied Research Center, Tabriz University of Medical Sciences, Tabriz, Iran*

ARTICLE INFO

Article history:
Received: 2022-05-29
Accepted: 2022-07-24
Available online: 2022-07-31

Keywords:
Graphene Oxide,
Bone Scaffold,
Regeneration,
Hydroxyapatite

ABSTRACT

Bone tissue engineering requires approaches to provide a suppression/promotion environment for the bone growth. Scaffold biomaterials have profound regulatory effects on the functionality of mesenchymal stem cells (MSCs). In the present study, the three-component bioceramic of selenium/reduced graphene oxide/hydroxyapatite (Se/RGO/HA) was developed and its performance to repair bone defects was compared to that of HA. The Se/RGO/HA nanocomposite scaffold was synthesized using the chemical bath technique, characterized by the X-ray diffraction spectra, field emission scanning electron microscopy, energy dispersion X-ray spectrometery, and Fourier transform infrared spectroscopy analyses. Human adipose-derived MSCs (hAD-MSCs) were used to investigate the in-vitro osteogenic properties of the Se/RGO/HA scaffold. The effect of the combined scaffold on the cell proliferation was analyzed by the MTT assay. Cell adhesion behaviors were evaluated using the optical microscopy and SEM. The osteogenic properties of the Se/RGO/HA scaffold were examined by the measurement of the alkaline phosphatase (ALP) activity and western blotting technique. The hAD-MSCs proliferation for HA and the Se/RGO/HA nanocomposite were 2 ± 0.1 and 1.1 ± 0.05 respectively. The Se/RGO/HA nanocomposite had cytotoxic effects on the KHOS-240S cancer cells. Additionally, good cell attachment and osteoblast-like morphology were characterized on the designed scaffold. The ALP activity and mineralization potential of cells seeded on Se/RGO/HA were higher than those seeded on HA. The Osteocalsin protein for Se/RGO/HA and HA were 64 ± 1 and 12 ± 0.1 respectively. Furthermore, the expression of Osteocalcin, a bone-specific protein, was synergistically increased by the incorporation of Se and RGO into HA. In conclusion, the presence of RGO inside Se could significantly increase the positive effects of HA on the osteogenic potential of hAD-MSCs.

DOI: 10.22034/ijche.2022.344213.1439 URL: http://www.ijche.com/article_154282.html

[*]Corresponding author: y.beygi@azaruniv.ac.ir (Y. Beygi-Khosrowshahi)

1. Introduction

The regeneration of the irreparably defected bones that are the main causes of functional disabilities and cosmetic problems remains a great challenge in medicine. Congenital anomalies, biochemical disorders, trauma, infections, and tumor resection are possible reasons for bone segmental defects [1-3]. In the last decades, bone tissue engineering (BTE) using a key triad of tissue building (scaffold, cells, and signaling molecules) provides efficient regeneration opportunities [4, 5]. Human mesenchymal stem cells (hMSCs) are highly potential cell sources to promote BTE, however, the controlled preferential direction of their differentiation along bone cells is still in progress. Scaffold is a structural support for the cell seeding, inclusion of growth factors, and domination of the newly formed tissue [6, 7]. Due to mimicking the native bone function, scaffolds play vital roles in the field of BTE. A variety of materials, natural or synthetic, has been considered to fabricate ideal scaffolds with the osteoconductive capacity. Among them, the bio-inspired ceramic of hydroxyapatite [HA, $Ca_{10}(PO_4)_6(OH)_2$] has attracted much attention due to its excellent biocompatibility, osteoconductivity, thermodynamic stability in physiological conditions, and ability to directly bond and integrate with the natural bone tissue [8-11]. However, the poor mechanical strength, brittle behavior, and weak wear resistance are the major obstacles for the clinical use of HA as bone scaffolds. One promising approach to solve these problems is using graphene and its derivatives such as graphene oxide (GO) and reduced graphene oxide (RGO). Graphene-based materials possess unique chemical, mechanical, electrical, optical, and thermal properties. They are biocompatible and bioactive materials capable of promoting the osteogenic differentiation and cell proliferation as well [12-17]. Selenium (Se) is an essential trace element that plays an important role in the biochemistry of bone [18, 19]. Se presents reactive oxygen species (ROS) scavenging, antibacterial, and anticancer activity in the human body and playes a significant role in the expansion and restoration of the antioxidative capacity of MSCs [20-23].

In one of our previous studies it was demonstrated that the Se-doped HA nanocomposite (Se/HA) could induce synergistic proliferative and osteoconductive effects on human adipose-derived MSCs (hAD-MSCs) [24]. In spite of the potential tissue engineering applications of graphene-based materials, just a little information is available about their osteogenic activity in the form of composite particles.

Therefore, investigating the synergistic effect of RGO beside the Selenium and Hydroxyapatite could be a novel scaffold for bone tissue engineering. In the following study, Se/RGO/HA nanocomposite is synthesized using the chemical bath deposition (CBD) method and characterized by the X-ray diffraction (XRD), Field emission scanning electron microscopy (FE-SEM), Energy dispersive X-ray spectroscopy (EDX), and Fourier transform infrared spectroscopy (FT-IR). Cell responses on Se/RGO/HA were analyzed in terms of adhesion, proliferation, and osteogenic differentiation using hAD-MSCs.

2. Materials and methods

2.1. Materials

The human adipose-derived mesenchymal stem cells (hAD-MSCs) were prepared from the Iranian Biological Resource Center

(Tehran, Iran). The Selenium dioxide (SeO_2) powder, Trypan blue solution, Graphene powder and MTT salt were purchased from Sigma-Aldrich (St. Louis, MO, USA). All cell culture components were obtained from Gibco (Life Technologies Ltd., UK). Other chemicals were acquired from Merck (Kenilworth, NJ, USA).

2.2. Preparation of RGO nanosheets

GO was synthesized from the expanded graphite using the modified Hummers and Offeman method. As a starting material, a small amount of graphite was used and placed into a beaker and heated for several seconds in an oven. GO nanosheets were obtained after suction drying over 12 h. For the reduction process, the synthesized GO was first sonicated in deionized (DI) water for several hours. Then Hydrazine hydrate was added to the suspension and the reaction proceeded at 100 °C for a 1 day period. Afterward, the suspension was filtered and washed with the DI water/ethanol solution several times. Finally, the RGO nanosheets were prepared after drying in a vacuum oven.

2.3. Synthesis of the Se/RGO/HA nanocomposite

Natural HA was extracted from bovine bones. Se was doped into the HA matrix according to the procedure reported in one of our earlier works [24]. Briefly, the HA extract and SeO_2 powder with a 1:1 molar ratio were mechanically alloyed for 20 h at 300 rpm. The resultant was heat-treated at 800 °C to obtain the Se/HA nanocomposite in the form of a white powder.

To prepare the Se/RGO/HA nanocomposite, Se/HA nanoparticles were first suspended in DI water and then mixed with a colloidal dispersion of RGO nanosheets in a 1:1 weight ratio. Then, the mixed colloidal dispersion was vortexed vigorously for 10 min. Finally, the solvent was allowed to be air-dried slowly overnight at room temperature to give the Se/RGO/HA nanocomposite.

3. Characterization

3.1. XRD

The crystal structure of synthesized compounds was characterized by an X-ray diffractometer (Advance D8, Bruker, Germany). Diffractograms were taken under the incident Cu Kα radiation (λ = 1.5406 Å) with a 2θ scale of 20-60° and a scan speed of 4°/min. The diffraction data were collected at an operational voltage/amperage of 35 kV/15 mA.

3.2. FE-SEM/EDX

The imaging technique of FE-SEM (Philips, CM 20, Netherland) was applied to determine the particle shape and size of the Se/RGO/HA nanocomposite. Before photographing, the surface of the sample was coated with a thin layer of gold. The beam electrons were accelerated by a voltage of 20 kV.

The elemental analysis of the nanocomposite sample was performed using EDX which is in conjunction with FE-SEM.

3.3. FT-IR

The analytical technique of FT-IR (4600 unicam, JASCO, Tokyo, Japan) was benefitted from to identify the functional groups existing in the nanocomposite scaffold. The pellet of the sample was prepared using potassium bromide as a transparent carrier. The infrared absorbance was recorded at 2.5-25 μm wavelength.

4. Cell culture

The present study was accomplished to assess the osteoconductive potential of the

Se/RGO/HA bioceramic compared to that of HA. The cell culture evaluation was performed using 2 mg of the sample and 2.5×10^5 hAD-MSCs/wall in a 24-well plate. First, samples were sterilized and washed with the EtOH solution (70 %) and phosphate buffered saline (PBS) respectively. Next, the cells were seeded using the complete medium of DMEM/F12 supplemented with 10% of the fetal bovine serum (FBS) and 1% of pen-strep antibiotics. Finally, the plates were incubated in a humidified incubator at 37 °C and 5 % of CO_2. The media were replaced with fresh ones every 48 h.

4.1. Analysis of the metabolic activity

An MTT assay was conducted to determine the metabolic activity of cells as a measure of the cellular proliferation. First, the stock solution was prepared by adding 1 ml of PBS to 5 mg of MTT (3-(4,5-dimethylthiazol-2-yl)-2, 5-diphenyl tetrazolium bromide). The MTT working solution was made up as a 10X stock solution using the DMEM/F12 medium. At the next stage, 1 ml of the MTT reagent was added to each well and incubated for 2 h. The assay was proceeded by the supernatant removal and formazan dissolution in 1 ml of isopropanol with a 10 % Triton X-100 and 0.1M HCl. Finally, a homogenous colored solution (200 µl) was transferred to a 96-well plate and the optical density (OD) was read at 570 nm using a microplate reader (Elx808, BioTek, USA).

4.2. Analysis of the cell-substrate adhesion

The cell-scaffold interface was visualized by the optical microscopy (BioTek-1X832-Desk, USA) and FE-SEM imaging techniques. For the FE-SEM analysis, the cell-seeded scaffold was first washed with PBS. Then, the sample was fixed in a formaldehyde solution (4 % (w/v) in PBS) at 4 °C for 20 min. Finally, fixed cells were washed with DI water.

4.3. Alkaline phosphatase activity

The early cell differentiation toward the Se/RGO/HA scaffold was characterized by the measurement of the ALP activity using the DGKC method [21]. After 3, 5, and 7 days, the cells were rinsed thrice with PBS and lysed in the lysis solution. Then, the cells were incubated at 37 °C for 30 min and kept at 4 °C overnight. Afterward, the cells were scratched and transferred into a tube for centrifugation (12,000 rpm, 10 min). Finally, the cell lysates were mixed with p-nitrophenyl phosphate, followed by the incubation in the dark (1 h, 25 °C). The ALP activity was measured at the 405 nm absorbance using a fluorescence microscope (Cytation 5, BioTek, USA).

4.4. Western blotting

After 7 days, the cells were rinsed twice in ice-cold PBS and treated with the lysis buffer. Cell debris were pelleted by centrifuging (12000 rpm, 10 min), and the concentration of the extract protein was measured using the Bradford protein assay. The extract was separated by the SDS-PAGE gel and transferred to a PVDF membrane using a transfer buffer. Then, the membrane was blocked with a 5 % skimed milk in TBST for 45 min (25 °C), probed with primary antibodies overnight (4 °C), and incubated with Anti Rabbit antibody (1:1000) for 75 min (25 °C). Finally, protein bands were visualized using an enhanced chemiluminescent reagent kit.

5. Results and discussion

5.1. Characterization of the Se/RGO/HA nanocomposite

5.1.1. XRD analysis

XRD is a powerful characterization technique used to determine the phase composition, average particle size, and crystallographic structure. The XRD analysis demonstrated that the peak pattern of the Se/RGO/HA nanocomposite is markedly similar to the diffraction pattern obtained for the HA (Figure 1). However, the intensity of peaks was slightly changed. This observation can be due to the amorphous nature of RGO which displays a broad and weak peak [25]. The XRD spectrum was also used to extract information on the particle size distribution. The average crystallite size of Se/RGO/HA particles was found to be 76 nm using the Debey-Scherrer formula ($D = k\lambda/\beta\cos\theta$).

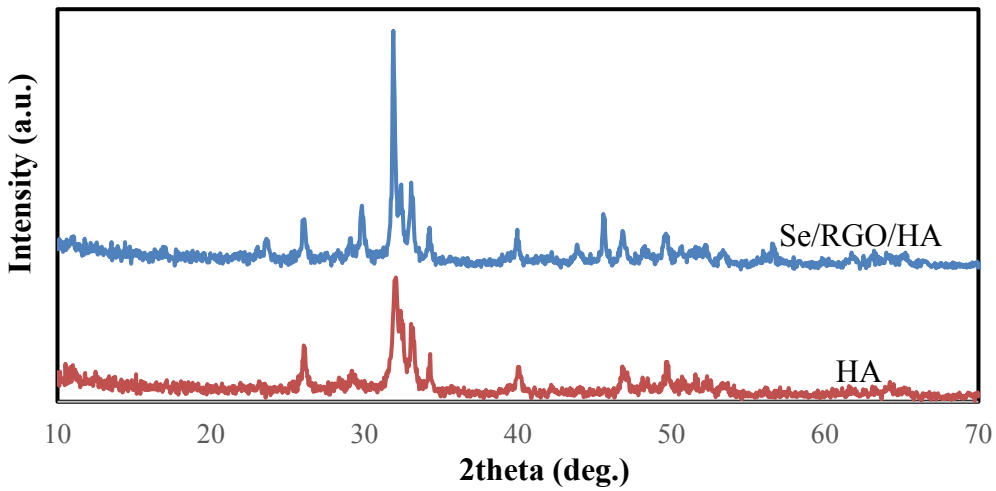

Figure 1. XRD patterns of HA and Se/RGO/HA scaffolds.

5.1.2. FT-IR

The results of XRD and EDX were further confirmed by the FT-IR analysis (Figure 2). By comparing the FT-IR diagrams, it is obvious that RGO sheets were successfully incorporated into the reported Se/HA structure [24]. The Se/RGO/HA scaffold displays a typical absorption band near 1600 cm^{-1}. This band is associated with the skeletal vibration of aromatic C=C group present in RGO. A very broad peak appeared in the 3100-3600 cm^{-1} region which corresponds to the hydrogen bonding interaction between the –OH groups of HA and O-containing groups of RGO (e.g., –OH, –CO–, –COOH and –O–) [17].

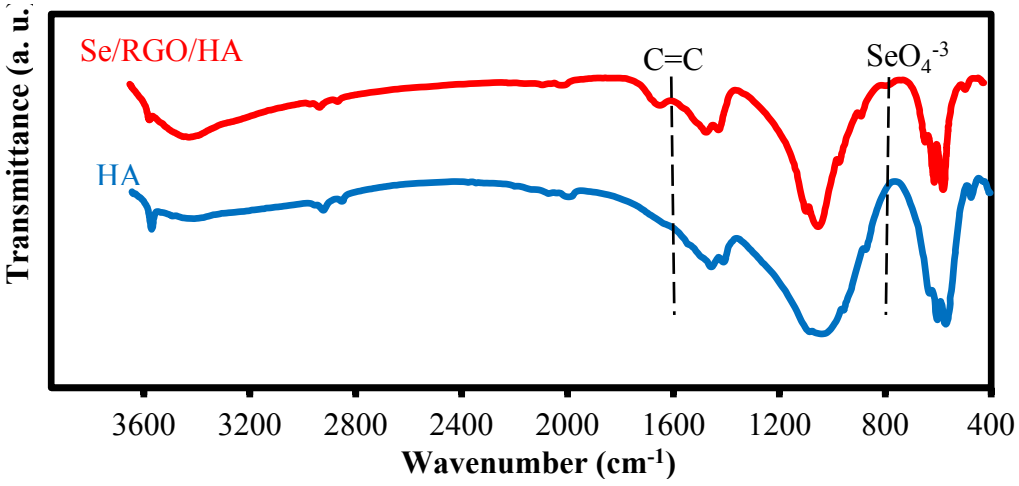

Figure 2. FTIR spectra of HA and Se/RGO/HA scaffolds.

5.2. Effect of the Se/RGO/HA nanocomposite on the cell viability

The tetrazolium salt-based assay (MTT) is the most commonly used assay to evaluate the cell viability. In this colorimetric method, the viable cells with active metabolism enzymatically reduce the yellow tetrazolium salt to purple formazan crystals. The darker the formazan solution, the greater the number of viable cells. According to the results illustrated in Figure 3a, hAD-MSCs represent higher growth capacity of the Se/RGO/HA scaffold compared to HA. The presence of Se and RGO in the HA structure leads to a synergistically increased the MSCs proliferation ($p < 0.05$). Furthermore, there is an ascending trend in the cell proliferation during the 7-day culture period. The improved proliferative capacity in response to RGO was consistent with the previous findings. Several studies have shown that graphene-based materials promote the MSCs proliferation [26].

Furthermore, the cytotoxicity and potential anticancer effect of the fabricated Se/RGO/HA was tested against a Human Bone Osteosarcoma cell line (KHOS-240S). As shown, the growth of cancer cells was predominantly inhibited on the engineered scaffold, while it follows a rising trend of HA after the incubation for 48 h (Figure 3b). Therefore, it seems that Se/RGO/HA can serve as a bifunctional scaffold with the ability of the concentration tumor suppression and bone restoration.

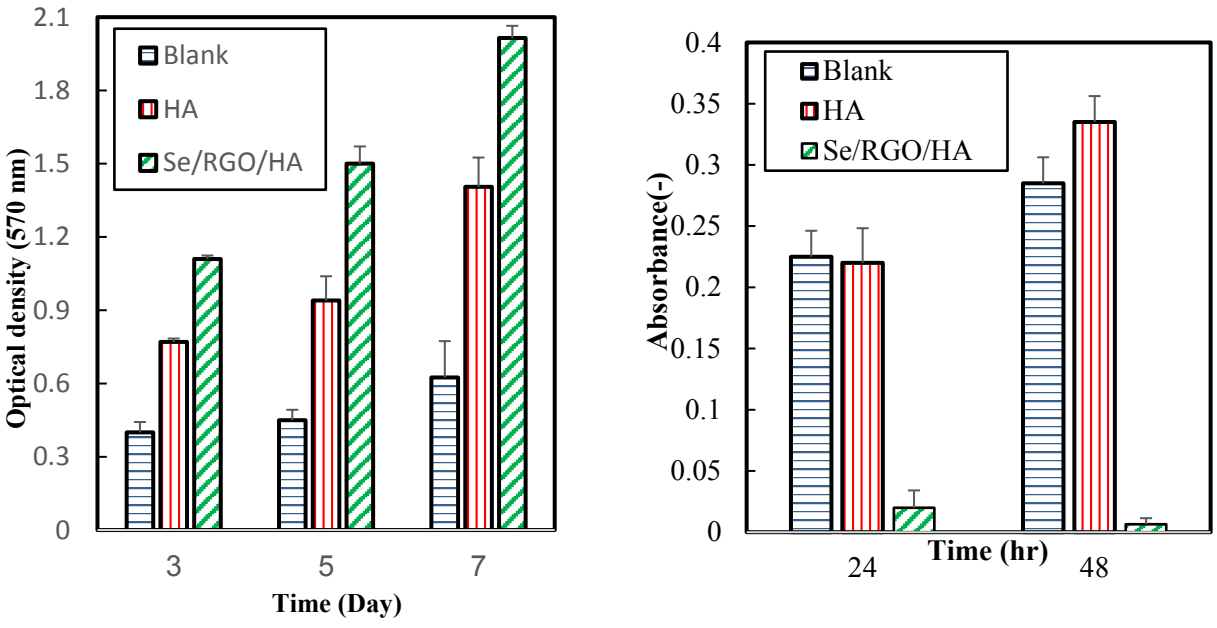

(a) (b)

Figure 3. MTT test for (a) hAD-MSCs in HA and Se/RGO/HA culture media on days 3, 5, and 7, (b) the KHOS-240S cell line after 24 and 48 h.

5.3. Effect of the Se/RGO/HA nanocomposite on the cell adhesion behavior

The chemical composition and physical property of scaffolds play vital roles in cell responses through cell-surface interactions. The optical microscopic imaging of the culture media-Se/RGO/HA interface exhibited the excellent accumulative behavior of hAD-MSCs and osteoblast-like

morphology toward the Se/RGO/HA scaffold (Figure 4a).

The adhesion behavior of hAD-MSCs in contact with the Se/RGO/HA scaffold was further examined by the FE-SEM imaging (Figure 4b). As depicted, the Se/RGO/HA nanocomposite possesses excellent biocompatibility with hAD-MSCs. The cells exhibit suitable cell-adhesion behavior on the designed scaffold. A number of studies have shown that graphene-based coatings provide non-cytotoxic surfaces and allow the successful adhesion of MSCs [27].

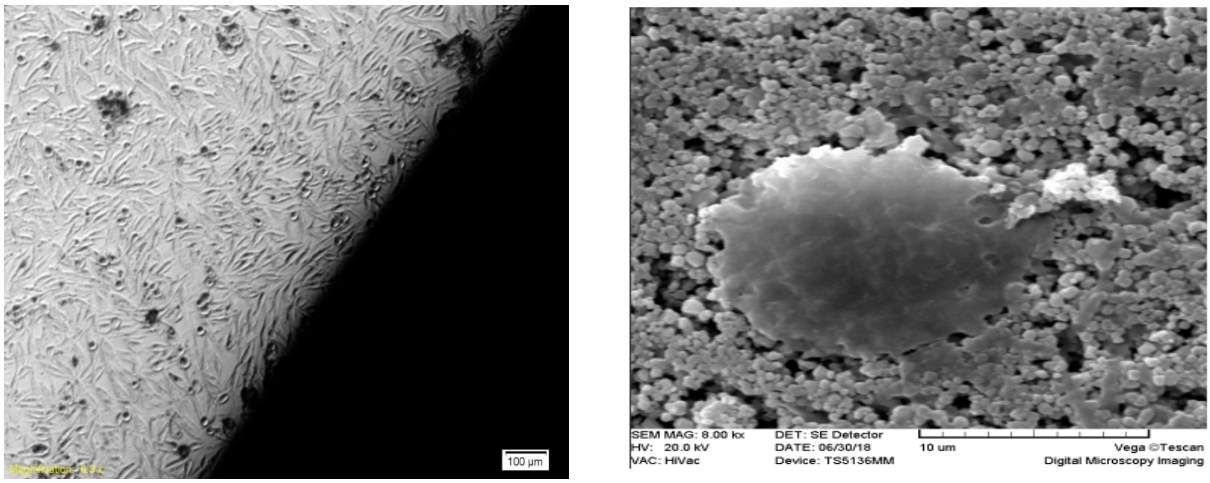

(a) (b)

Figure 4. (a) Optical microscopy and (b) Fe-SEM micrographs of the cross section of hAD-MSCs with the Se/RGO/HA scaffold on day 3.

5.4. Effect of the Se/RGO/HA nanocomposite on the ALP activity

ALP is a phenotypic marker of osteoblast cells that is abundantly synthesized during the early stage of the osteogenic differentiation [28, 29]. It is an essential enzyme to supply phosphate for the bone mineral formation [30]. In the current study, the ALP activity of cells grown on the Se/RGO/HA scaffold was evaluated over 7 days and plotted in Figure 5. In comparison with HA, the Se/RGO/HA scaffold could synergistically promote the ALP activity of cells on days 3, 5, and day 7 ($p < 0.05$). Acceding to the results, Se and RGO had additive effects on the ALP activity of hAD-MSCs. Furthermore, the ALP activity of cells increased by increasing the incubation time. In a study performed by Jin et al., a similar osteogenic property was reported for the RGO material. According to their result, RGO has a stimulating effect on the ALP activity of MSCs [31]. In another study, Nie et al. reported improved the ALP activity of MSCs on the combined HA/RGO scaffold [32].

5.5. Effect of the Se/RGO/HA nanocomposite on the protein expression

The transition of MSCs to osteoblasts is characterized by the synthesis and secretion of bone ECM proteins. Osteocalcin (OCN) is a calcium-binding protein which is found abundantly in the bone matrix [36, 37]. At the end of study, the western blotting technique was applied to detect and quantify the OCN protein expression in the cells grown on the Se/RGO/HA scaffold. As illustrated in Figure 6, the OCN expression showed an upward trend in cells cultured in a group with Se/HA. According to the results, a three-component

composite of Se/RGO/HA induced a synergistic effect on the hAD-MSCs differentiation to promote the bone reconstruction ($p < 0.05$). These results are in conformity with those of previous studies, which suggested that RGO could induce the osteogenic differentiation of MSCs [27, 35].

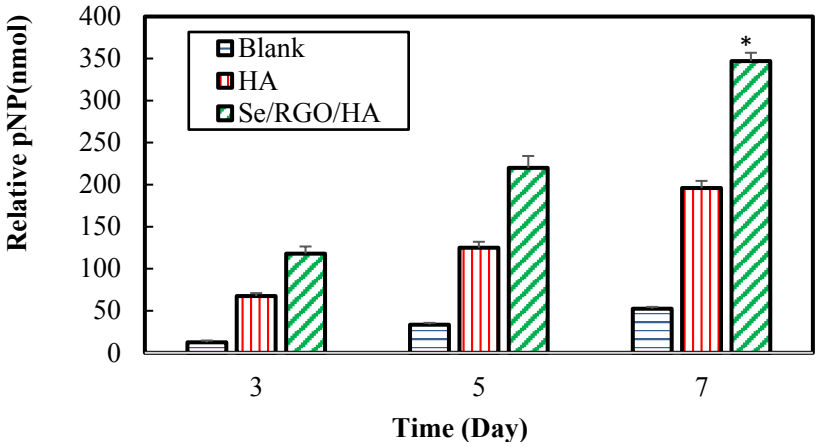

Figure 5. Alkaline phosphatase activity of hAD-MSCs in HA and Se/RGO/HA culture media on days 3 and 7.

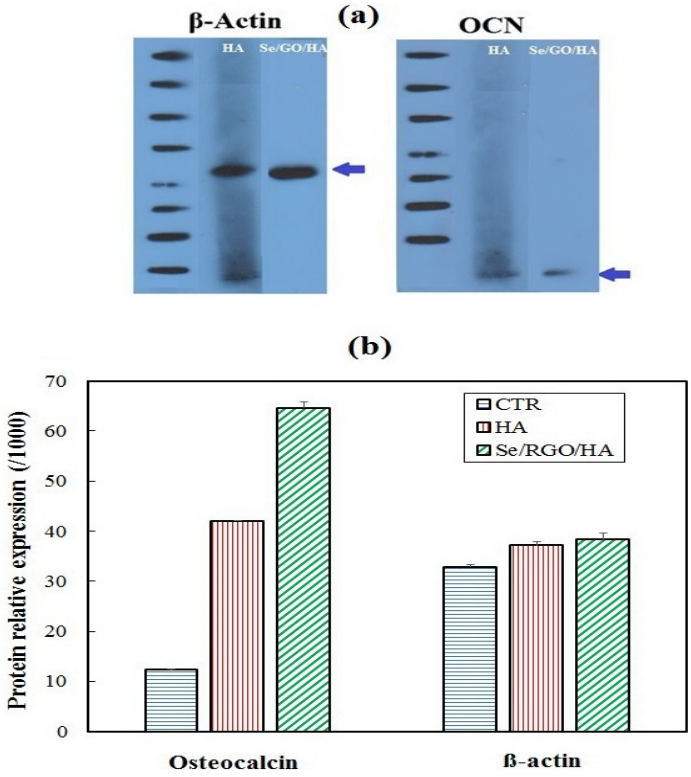

Figure 6. (a) Western blot tests for Osteocalcin (OCN) and Beta-actin proteins in hAD-MSCs, (b) Quantity evaluation of the OCN protein on day 7.

6. Conclusions

In conclusion, the Se/RGO/HA nanocomposite as the bone scaffold was found to be more favorable than HA. The Se/RGO/HA scaffold presented good biocompatibility, and the hAD-MSCs

displayed suitable cell-adhesion behavior and osteoblast-like morphology on the prepared scaffold. The hAD-MSCs proliferation for HA, Se/HA and the Se/RGO/HA nanocomposite were 2 ± 0.1, 1.45 ± 0.2 and 1.1 ± 0.05 respectively.

The Osteocalsin protein for HA, Se/HA and Se/RGO/HA were 64 ± 1, 41 ± 0.1 and 12 ± 0.1 respectively. These results revealed that the presence of Se and RGO in the HA structure could induce a synergistically increased cell proliferation on the MSCs cells. Moreover, the expression of Osteocalcin, a bone-specific protein, was synergistically increased by incorporation of Se and RGO into HA. In conclusion, the presence of RGO inside Se could significantly increase positive effects of HA on the osteogenic potential of hAD-MSCs.

Furthermore, the results of osteogenic differentiation demonstrated the synergistically enhanced ALP activity and protein expression of OCS on the Se/RGO/HA scaffold compared to HA.

References

[1] Chaparro, O. and Linero, I., "Regenerative medicine: A new paradigm in bone regeneration", Advanced techniques in bone regeneration, Rozim Zorzi, A. and de Miranda, J. B. edition, 1st ed., Intechopen, p. 253 (2016).

[2] Kiernan, C., Knuth, C. and Farrell, E., "Chapter 6 - Endochondral ossification: Recapitulating bone development for bone defect repair", Developmental biology and musculoskeletal tissue engineering, Stoddart, M. J., Craft, A. M., Pattappa, G. and Gardner, O. F. W. edition, Academic Press, Boston, p. 125 (2018).

[3] Awad, H. A., O'Keefe, R. J. and Mao, J. J., "Chapter 81 - Bone tissue engineering", Principles of tissue engineering, Lanza, R., Langer, R., Vacanti, J. P. and Atala, A. edition, Fifth ed., Academic Press, p. 1511 (2020).

[4] Hadi, F., Awan, D., Tahir Maqbool, D., Shehzadi, S., Javed, S. and Kiran, K., "Stem cells, scaffolds and signaling molecules as a multidisciplinary", *Approach for Tissue Engineering*, **6**, 132018014 (2018).

[5] Murphy, C. M., O'Brien, F. J., Little, D. G. and Schindeler, A., "Cell-scaffold interactions in the bone tissue engineering triad", *Eur. Cell Mater.*, **26** (4), 120 (2013).

[6] Eltom, A., Zhong, G. and Muhammad, A., "Scaffold techniques and designs in tissue engineering functions and purposes: A review", *Advances in Materials Science and Engineering*, 3429527 (2019). (https://doi.org/10.1155/2019/3429527).

[7] Carvalho, J., Carvalho, P., Gomes, D. and Goes, A., "Innovative strategies for tissue engineering", Advances in biomaterials science and biomedical applications, InTech, Rijeka, Croatia, p. 295 (2013).

[8] Baino, F., Novajra, G. and Vitale, B. C., "Bioceramics and scaffolds: A winning combination for tissue engineering", *Frontiers in Bioengineering and Biotechnology*, **3** (202), (2015).

[9] Gervaso, F., Scalera, F., Kunjalukkal, P. S., Sannino, A. and Licciulli, A., "High-performance hydroxyapatite scaffolds for bone tissue engineering applications", *International Journal of Applied Ceramic Technology*, **9** (3), 507 (2012).

[10] Gao, C., Deng, Y., Feng, P., Mao, Z., Li,

P. and Yang, B., "Current progress in bioactive ceramic scaffolds for bone repair and regeneration", *International Journal of Molecular Sciences*, **15** (3), 4714 (2014).

[11] Orozco-Díaz, C. A., Moorehead, R., Reilly, G. C., Gilchrist, F. and Miller, C., "Characterization of a composite polylactic acid-hydroxyapatite 3D-printing filament for bone-regeneration", *Biomedical Physics & Engineering Express*, **6** (2), 025007 (2020).

[12] Nayak, T. R., Andersen, H., Makam, V. S., Khaw, C., Bae, S. and Xu, X., "Graphene for controlled and accelerated osteogenic differentiation of human mesenchymal stem cells", *ACS Nano*, **5** (6), 4670 (2011).

[13] Park, J., Park, S., Ryu, S., Bhang, S. H., Kim, J. and Yoon, J. K., "Graphene–regulated cardiomyogenic differentiation process of mesenchymal stem cells by enhancing the expression of extracellular matrix proteins and cell signaling molecules", *Advanced Healthcare Materials*, **3** (2), 176 (2014).

[14] Lee, W. C., Lim, C. H. Y., Shi, H., Tang, L. A., Wang, Y. and Lim, C. T., "Origin of enhanced stem cell growth and differentiation on graphene and graphene oxide", *ACS Nano*, **5** (9), 7334 (2011).

[15] Yoon, H. H., Bhang, S. H., Kim, T., Yu, T., Hyeon, T. and Kim, B. S., "Dual roles of graphene oxide in chondrogenic differentiation of adult stem cells: Cell-adhesion substrate and growth factor-delivery carrier", *Advanced Functional Materials*, **24** (41), 6455 (2014).

[16] Ku, S. H. and Park, C. B., "Myoblast differentiation on graphene oxide", *Biomaterials*, **34** (8), 2017 (2013).

[17] Lee, J. H., Shin, Y. C., Lee, S. M., Jin, O. S., Kang, S. H. and Hong, S. W., "Enhanced osteogenesis by reduced graphene oxide/hydroxyapatite nanocomposites", *Scientific Reports*, **5** (1), 1 (2015).

[18] Rayman, M. P., "The importance of selenium to human health", *The Lancet*, **356** (9225), 233 (2000).

[19] Roman, M., Jitaru, P. and Barbante, C., "Selenium biochemistry and its role for human health", *Metallomics*, **6** (1), 25 (2014).

[20] Korowash, S., Burdzinska, A., Pędzisz, P., Dąbrowski, F, Mostafa, A. M. and Abdel-Razik, A., "Selenium substituted hydroxyapatite nanoparticles and their in vitro interaction on human bone marrow- and umbilical cord-derived mesenchymal stem cells", *Interceram-International Ceramic Review*, **66** (6), 244 (2017).

[21] Tinggi, U., "Selenium: Its role as antioxidant in human health", *Environmental Health and Preventive Medicine*, **2** (13), 102 (2008).

[22] Rodríguez-Valencia, C., López-Álvarez, M., Cochón-Cores, B., Pereiro, I., Serra, J. and Gonzálezm P., "Novel selenium-doped hydroxyapatite coatings for biomedical applications", *Journal of Biomedical Materials Research, Part A*, **101** (3), 853 (2013).

[23] Park, J., Lee, J. H., Yoon, B. S., Jun, E. K., Lee, G. and Kim, I. Y., "Additive effect of bFGF and selenium on expansion and paracrine action of human amniotic fluid-derived mesenchymal stem cells", *Stem Cell Research & Therapy*, **9** (1), 293 (2018).

[24] Zakhireh, S., Adibkia, K., Khosrowshahi, Y. and Barzegar-Jalali, M., "Osteogenesis promotion of selenium-doped hydroxyapatite for application as

bone scaffold", *Biological Trace Element Research*, **199**, 1802 (2021).

[25] Lee, J. H., Shin, Y. C., Lee, S. M., Jin, O. S., Kang, S. H. and Hong, S. W., "Enhanced osteogenesis by reduced graphene oxide/hydroxyapatite nanocomposites", *Scientific Reports*, **5** (1), 18833 (2015).

[26] Gurunathan, S. and Kim, J. H., "Synthesis, toxicity, biocompatibility, and biomedical applications of graphene and graphene-related materials", *International Journal of Nanomedicine*, **11**, 1927 (2016).

[27] Dubey, N., Bentini, R., Islam, I., Cao, T., Castro, N. A. H. and Rosa, V., "Graphene: A versatile carbon-based material for bone tissue engineering", *Stem Cells International*, (2015).

[28] Mizerska-Kowalska, M., Sławińska-Brych, A., Kaławaj, K., Żurek, A., Pawińska, B. and Rzeski, W., "Betulin promotes differentiation of human osteoblasts in vitro and exerts an osteoinductive effect on the hFOB 1.19 cell line through activation of JNK, ERK1/2 and mTOR kinases", *Molecules*, **24** (14), 2637 (2019).

[29] Beloti, M. M. and Rosa, A. L., "Osteoblast differentiation of human bone marrow cells under continuous and discontinuous treatment with dexamethasone", *Brazilian Dental Journal*, **16** (2), 156 (2005).

[30] Blair, H. C., Larrouture, Q. C., Li, Y., Lin, H., Beer-Stoltz, D. and Liu, L., "Osteoblast differentiation and bone matrix formation in vivo and in vitro", *Tissue Engineering, Part B: Reviews*, **23** (3), 268 (2017).

[31] Jin, L., Lee, J. H., Jin, O. S., Shin, Y. C., Kim, M. J. and Hong, S. W., "Stimulated osteogenic differentiation of human mesenchymal stem cells by reduced graphene oxide", *Journal of Nanoscience and Nanotechnology*, **15** (10), 7966 (2015).

[32] Nie, W., Peng, C., Zhou, X., Chen, L., Wang, W. and Zhang, Y., "Three-dimensional porous scaffold by self-assembly of reduced graphene oxide and nano-hydroxyapatite composites for bone tissue engineering", *Carbon*, **116**, 325 (2017).

[33] Pan, H., Jiang, S., Zhang, T. and Tang, R., "In situ solution study of calcium phosphate crystallization kinetics", Methods in enzymology, 532, Academic Press, p. 129 (2013).

[34] Baino, F., "Ceramics for bone replacement: Commercial products and clinical use", Advances in ceramic biomaterials, Woodhead Publishing, p. 249 (2017).

[35] Jin, L., Lee, J. H., Jin, O. S., Shin, Y. C., Kim, M. J. and Hong, S. W., "Stimulated osteogenic differentiation of human mesenchymal stem cells by reduced graphene oxide", *Journal of Nanoscience and Nanotechnology*, **15** (10), 7966 (2015).

[36] Florencio-Silva, R., Sasso, G. R., Sasso-Cerri, E., Simões, M. J. and Cerri, P. S., "Biology of bone tissue: Structure, function, and factors that influence bone cells", *BioMed Research International*, (2015).

[37] Patti, A., Gennari, L., Merlotti, D., Dotta, F. and Nuti, R., "Endocrine actions of osteocalcin", *International Journal of Endocrinology*, **2013**, 846480 (2013).